

Earth's Future

RESEARCH ARTICLE

10.1029/2023EF003684

Key Points:

- Historical sea-level changes in the Indo-Pacific warm pool region are attributed using large-ensemble climate model simulations
- The role of greenhouse gas forcing on historical sea-level changes is dominant, but the time of emergence varies regionally
- Tropical Indian Ocean dynamics played a key role in controlling historical sea-level changes in the Indo-Pacific warm pool region

Supporting Information:

Supporting Information may be found in the online version of this article.

Correspondence to:

D. Samanta,
dhruba@ntu.edu.sg

Citation:








Samanta, D., Vairagi, V., Richter, K., McDonagh, E. L., Karnauskas, K. B., Goodkin, N. F., et al. (2024). The role of anthropogenic forcings on historical sea-level change in the Indo-Pacific warm pool region. *Earth's Future*, 12, e2023EF003684. <https://doi.org/10.1029/2023EF003684>

Received 24 MAR 2023

Accepted 10 JAN 2024

© 2024. The Authors. Earth's Future published by Wiley Periodicals LLC on behalf of American Geophysical Union. This is an open access article under the terms of the [Creative Commons Attribution-NonCommercial-NoDerivs License](#), which permits use and distribution in any medium, provided the original work is properly cited, the use is non-commercial and no modifications or adaptations are made.

The Role of Anthropogenic Forcings on Historical Sea-Level Change in the Indo-Pacific Warm Pool Region

Dhrubajyoti Samanta¹ , Vedant Vairagi^{1,2}, Kristin Richter³ , Elaine L. McDonagh^{3,4} , Kristopher B. Karnauskas^{5,6} , Nathalie F. Goodkin⁷ , Lock Yue Chew⁸ , and Benjamin P. Horton^{1,9} 

¹Earth Observatory of Singapore, Nanyang Technological University, Singapore, Singapore, ²Now at University of Reading, Reading, UK, ³NORCE Norwegian Research Centre, Bjerknes Centre for Climate Research, Bergen, Norway, ⁴National Oceanography Centre, Southampton, UK, ⁵Department of Atmospheric and Oceanic Sciences, University of Colorado Boulder, Boulder, CO, USA, ⁶Cooperative Institute for Research in Environmental Sciences, University of Colorado Boulder, Boulder, CO, USA, ⁷Department of Earth and Planetary Sciences, American Museum of Natural History, New York, NY, USA, ⁸School of Physical and Mathematical Sciences, Nanyang Technological University, Singapore, Singapore, ⁹Asian School of the Environment, Nanyang Technological University, Singapore, Singapore

Abstract Detecting and attributing sea-level rise over different spatiotemporal scales is essential for low-lying and highly populated coastal regions. Using the Detection and Attribution Model Intercomparison Project (DAMIP) from the Coupled Model Intercomparison Project Phase 6, we evaluate the role of anthropogenic forcing in sea-level change in the historical (1950–2014) period in the Indo-Pacific warm pool region. We use three models that have at least 10 ensemble members, corresponding to different DAMIP simulations. We determined the changes in regional sea level from both natural and anthropogenic forcings. Our results demonstrate: (a) the emergence of an anthropogenic footprint on regional steric sea-level change has a large spatiotemporal diversity over the Indo-Pacific warm pool region with the earliest emergence in the western Indian Ocean; (b) a significant rise in dynamic sea level (DSL) (up to 25 mm) and thermosteric (up to 40 mm) sea level over the western Indian Ocean due to greenhouse gas forcing; (c) a positive Indian Ocean Dipole-like pattern in the DSL changes over the tropical Indian Ocean; (d) a significant increase in the halosteric contribution to sea-level rise in the Indo-Pacific warm pool region, and (e) a pronounced rise of manometric sea level (up to 20 mm) over shallow oceans and coastal regions in recent decades. These results provide a comprehensive spatiotemporal analysis of the attribution of anthropogenic factors to sea-level changes in the Indo-Pacific warm pool region.

Plain Language Summary Various natural and human-induced factors contribute to sea-level change, but separating their distinct impacts on a regional to local scale remains challenging. Here we use computer model simulations of global climate to detect and attribute historical sea-level changes (1950–2014) in the Indo-Pacific warm pool region to anthropogenic greenhouse gas and aerosol forcing versus natural forcing. We discovered that the historical rise in sea level is predominantly driven by the influence of greenhouse gases, although aerosols tend to moderate the rate of rise. Notably, the rate of sea-level rise and the time of emergence of anthropogenic signals vary spatially in the region. As an example, anthropogenic signals emerged earlier in the western Indian Ocean in the twentieth century than in the eastern Indian Ocean. Sea-level rise in the deeper oceans of the Indo-Pacific warm pool region is primarily governed by changes in ocean temperature (termed *thermosteric*) and salinity (*halosteric*). Conversely, in shallow regions such as over the maritime continent and continental shelves, sea-level rise is primarily a consequence of a local increase in ocean mass (*manometric*). Our study provides a better understanding of the attribution of regional sea-level changes in the recent past and their possible implications for the future.

1. Introduction

Improved knowledge of the forcings of past climate changes increases confidence in future projections (Tierney et al., 2020). This evolving science of climate change attribution improves our understanding of how the global climate system is changing and aids discussions about responsibility and accountability for the effects (Gillett et al., 2021; Hegerl & Zwiers, 2011; Stott et al., 2010). Sea-level rise is one of the most significant impacts of climate change (e.g., Horton et al., 2018). Changes in global and regional sea level are driven by a range of natural and anthropogenic forcings (Dangendorf et al., 2015; Kopp et al., 2015; Slangen et al., 2014). The

Intergovernmental Panel on Climate Change sixth assessment report suggests that there has been evidence of anthropogenic forcing on the two main contributors to the sea-level rise since 1950: thermal expansion of ocean water (i.e., thermosteric effect), and melting of glaciers and ice sheets (Fox-Kemper et al., 2021).

Prior research on attributing sea-level rise to anthropogenic forcing predominantly focuses on global mean sea level, which Tokarska et al. (2019) argued, along with ocean warming, is detectable over the historical period and attributable to anthropogenic forcings. On a longer timescale, Jevrejeva et al. (2009) evaluated the role of various natural and anthropogenic forcings on global sea level for the past 1,000 years based on a statistical model and argued that in the past 200 years, sea-level rise has been mostly associated with anthropogenic factors. Similarly, using optimal fingerprinting, Slangen et al. (2014) argued that anthropogenic forcings are required to explain the magnitude of the observed global mean thermosteric sea-level rise during 1957–2005. Expanding on those results and considering different forcings, Marzeion et al. (2014) found that the anthropogenic contribution to glacial mass loss has increased markedly over the past decades. Dangendorf et al. (2015) provided a significant anthropogenic footprint on global mean sea-level rise since 1900 by assessing the spectral properties of the slowly varying volumetric component and the rapidly changing atmospheric component. Finally, Walker et al. (2022) used proxy records spanning the common era (0–2000 CE) to show that the time of emergence of sea-level rise above pre-industrial rates is similar in timing to early ocean warming and glacier melt.

A limitation of sea-level attribution is the paucity of regional sea-level studies (Stammer et al., 2013; Walker et al., 2021). Regional sea level differs from the global mean because of changes in atmospheric and oceanic circulations, steric effects, vertical land motion from glacial isostatic adjustment, tectonics, sediment compaction, and gravitational, rotational and deformational responses to barystatic changes (Gregory et al., 2019; Horton et al., 2018; Milne et al., 2009; Stammer et al., 2013). Detecting anthropogenically forced signals on a regional scale is more challenging than on a global scale due to the varied expression of natural climate variability (e.g., Richter et al., 2020; Richter & Marzeion, 2014). Natural climate variability can emerge over multiple timescales without the influence of external forces from anthropogenic activities. For example, the regional sea level in the tropical Pacific Ocean is dominated by natural variability in the decadal timescale rather than external forcing (Meyssignac et al., 2012), specifically by the Pacific Decadal Oscillation (e.g., Hamlington, Strassburg, et al., 2014; Scafetta, 2014). Moreover, the absence of large ensemble simulations in the earlier generations of the Coupled Model Intercomparison Projects (CMIP) hampered regional sea-level attribution studies because of the uncertainties due to internal variability in the climate models (e.g., Frankignoul et al., 2017; Maher et al., 2019). Nevertheless, using observed and simulated geocentric sea-level change during 1993–2015, Richter et al. (2020) concluded that a forced signal can be detected globally and at all latitudes of each major ocean basin.

Here we examine regional sea-level attribution in the tropical Indo-Pacific, specifically the Indo-Pacific warm pool region (Figure 1; 25°S–25°N, 40°E–130°W). This region has a dense coastal population that is particularly vulnerable to sea-level rise (Figure 1a; Fox-Kemper et al., 2021). Over the satellite altimetry era, the Indo-Pacific warm pool region has experienced sea-level rise up to 6.4 mm/year, which is nearly double the global average (Figure 1a) of ~3.4 mm/year. Indeed, from 1993 to 2022, the warm pool region has exhibited one of the highest sea-level rise trends globally (Figure 1a). The Indo-Pacific warm pool region (Figures 1b and 1c) is characterized by a permanent sea surface temperature (SST) above 28°C and plays a crucial role in various ocean-atmosphere processes that are essential for the global water cycle (e.g., De Deckker, 2016; Weller et al., 2016). The Indo-Pacific warm pool area has expanded at a rate of 4×10^5 km² per year between 1981 and 2018 (Roxy et al., 2019) due to anthropogenic factors (Bai et al., 2022; Weller et al., 2016). This expansion is more than two-fold during 1993–2022 (Figures 1b and 1c), relative to the 1900–1980 climatology (Figure 1b), probably due to the increasing role of anthropogenic forcings in the region.

We attribute sea-level changes over the Indo-Pacific warm pool region during the historical period (1950–2014) to natural and anthropogenic forcings from the recent generation of climate models from CMIP Phase 6 (CMIP6; Eyring et al., 2016). The CMIP6 climate models realistically represent regional sea-level variability (Chen et al., 2023; Ferrero et al., 2021; Lyu et al., 2020; Sajidh & Chatterjee, 2023) and are widely used in attribution studies (e.g., Bai et al., 2022; Dong et al., 2021; Goodkin et al., 2021). We estimate the natural and anthropogenic contributions of historical sea-level change, considering temperature (termed thermosteric), salinity (termed halosteric), and local mass of the ocean per unit area (termed manometric) components. We also consider some possible physical mechanisms driving simulated dynamic sea level (DSL) change. We focus only on the oceanic

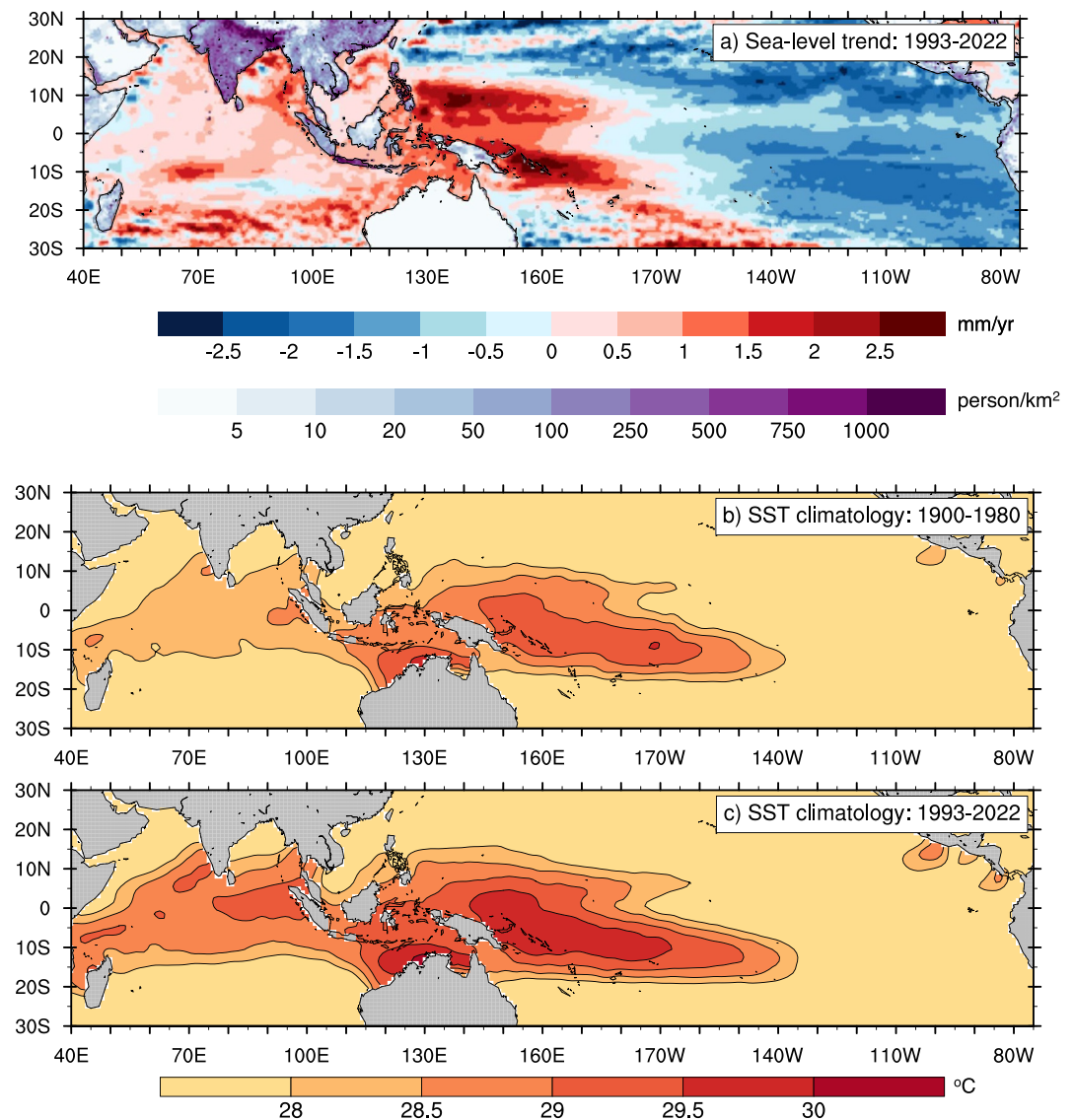


Figure 1. Association of higher sea-level trend, population density, and sea surface temperature (SST) changes over the Indo-Pacific region. (a) Sea-level trend from satellite observations during 1993–2022 relative to the global mean (shaded over oceans; in mm/year) and 2020 population density (shaded over land; in person/km²); (b) November–April SST climatology (in °C) during 1900–1980; (c) same as (b), but for 1993–2022. Global mean sea-level trend (3.4 mm/year) is subtracted in (a) to highlight the regional anomalies. Sea-level data is from two-satellite merged constellation (Copernicus Climate Change Service [C3S]) available from <https://cds.climate.copernicus.eu/cdsapp#!/dataset/satellite-sea-level-global?tab=form> and observed SST data is from HadISST1 product available from <https://www.metoffice.gov.uk/hadobs/hadisst/data/download.html>.

contributions to regional sea-level changes and do not consider contributions from the barystatic component, vertical land motion, or glacial isostatic adjustment.

2. Data and Methods

2.1. Observations and Climate Model Data

We use monthly gridded sea-level data (1993–2022) from satellite observations for the global oceans from the Copernicus Climate Change Service Climate Data Store at 0.25° × 0.25° horizontal resolution and gridded world

population data for 2020 (Warszawski et al., 2017) (Figure 1a). The SST is from the Hadley Center Sea Ice and Sea Surface Temperature data set (Rayner et al., 2003).

To evaluate the potential attribution of changing sea-level patterns to anthropogenic forcing, we utilize the Detection and Attribution Model Intercomparison Project (DAMIP; Gillett et al., 2016; see Table S1 in Supporting Information S1 for experiment details) from CMIP6 (Eyring et al., 2016). One of the objectives of DAMIP is to improve the estimation of natural and anthropogenic forcing to observed global warming at global and regional scales (Gillett et al., 2016). We select three climate models based on the availability of at least 10 common ensemble members across different forcing simulations: CanESM5 (hereafter CanESM; 30 ensembles), CNRM-CM6-1 (hereafter CNRM; 10 ensembles), and IPSL-CM6-LR (hereafter IPSL; 10 ensembles) (see Table S2 in Supporting Information S1 for details). We use the following variables available at monthly resolution from these climate models: global mean thermosteric sea level (*zostoga*), DSL (*zos*), sea-level pressure (*PSL*), zonal and meridional near-surface wind (*UAS*, *VAS*), three-dimensional potential temperature (*thetao*), and practical salinity (*so*). The DSL changes represent both local mass and density changes. The DSL is defined such that the global mean is zero at each time step.

The three selected models successfully reproduce many observed spatial patterns of the surface climate, interior ocean, atmosphere, and various modes of tropical climate variabilities (Bonnet et al., 2021; Swart et al., 2019; Voldoire et al., 2019). For example, Swart et al. (2019) showed the spectral peak of El Niño Southern Oscillation in CanESM historical ensemble members occurs every ~3–5 years, consistent with observations. CanESM represents SST teleconnection in the tropical Indian and Atlantic Oceans (Swart et al., 2019). These three models also incorporate realistic river runoff (Boucher et al., 2020; Swart et al., 2019; Voldoire et al., 2019).

The historical run includes all forcings, and the difference between simulations with historical forcings (HIS) and natural-only forcings (NAT) isolates the impact of all anthropogenic forcings (e.g., Ribes et al., 2015). We make the assumption of linear superposition following the below equation (Ribes et al., 2015).

$$\text{HIS} = \text{NAT} + \text{AER} + \text{GHG} \quad (1)$$

We identify specific drivers of anthropogenic changes using aerosol-only (AER) and greenhouse gas-only (GHG) forced runs. This assumes that forcings other than AER, GHG, and NAT have a negligible impact. Here we use a high number of ensembles from climate models because detection and attribution requires a proper estimation of the smallest amplitude signals (primarily NAT) (Ribes et al., 2015). Consideration of large ensemble experiments also reduces a climate model's internal variability about the ensemble mean (e.g., Yu et al., 2020). However, here we do not use any formal statistical assessment of detection and attribution, such as the optimal fingerprinting approach used in earlier studies (e.g., Bai et al., 2022; Slangen et al., 2014).

First, we remove the time-varying model drift of *zos* and *zostoga* based on the linear trend of pre-industrial control simulation, following Sen Gupta et al. (2013). Each scenario is presented herein as the ensemble mean of each model. We show the long-term changes in sea level in the historical period (1985–2014 minus 1950–1979) using annual mean data due to the dominant anthropogenic influence on the global climate in the second half of the twentieth century (e.g., Fox-Kemper et al., 2021), unless otherwise stated. Recent decades also exhibit a higher sea-level rise trend and more pronounced Indo-Pacific warm pool area expansion relative to 1950–1979 period (Figure S1 in Supporting Information S1; Hamlington, Leben, et al., 2014). Second, we evaluate the 30-year average, which largely removes the effect of interannual-to-decadal climate variabilities and the issues related to shorter time scales while detecting anthropogenic signals in sea-level change (Hamlington et al., 2021; Richter et al., 2020). Note that leaving a few years of buffer between the two periods (1950–1979 and 1985–2014) has a negligible impact on our results. The CMIP6 historical simulations end in December 2014.

The time evolution of DSL and associated near-surface changes are examined by area averaging over four key regions (Figure 2d): (a) western Indian Ocean (10°S–10°N, 50°E–70°E), (b) eastern Indian Ocean (10°S–EQ, 90°E–110°E), (c) South China Sea (5°N–15°N, 105°E–115°E), and (d) western Pacific Ocean (15°N–25°N, 125°E–135°E). The western and eastern Indian Ocean regions are typically considered to study the Indian Ocean Dipole (IOD, Hameed, 2018).

We display CanESM results in the main figures due to the availability of its large ensemble number and the availability of ocean bottom water pressure data to calculate manometric sea level. All results from the other two

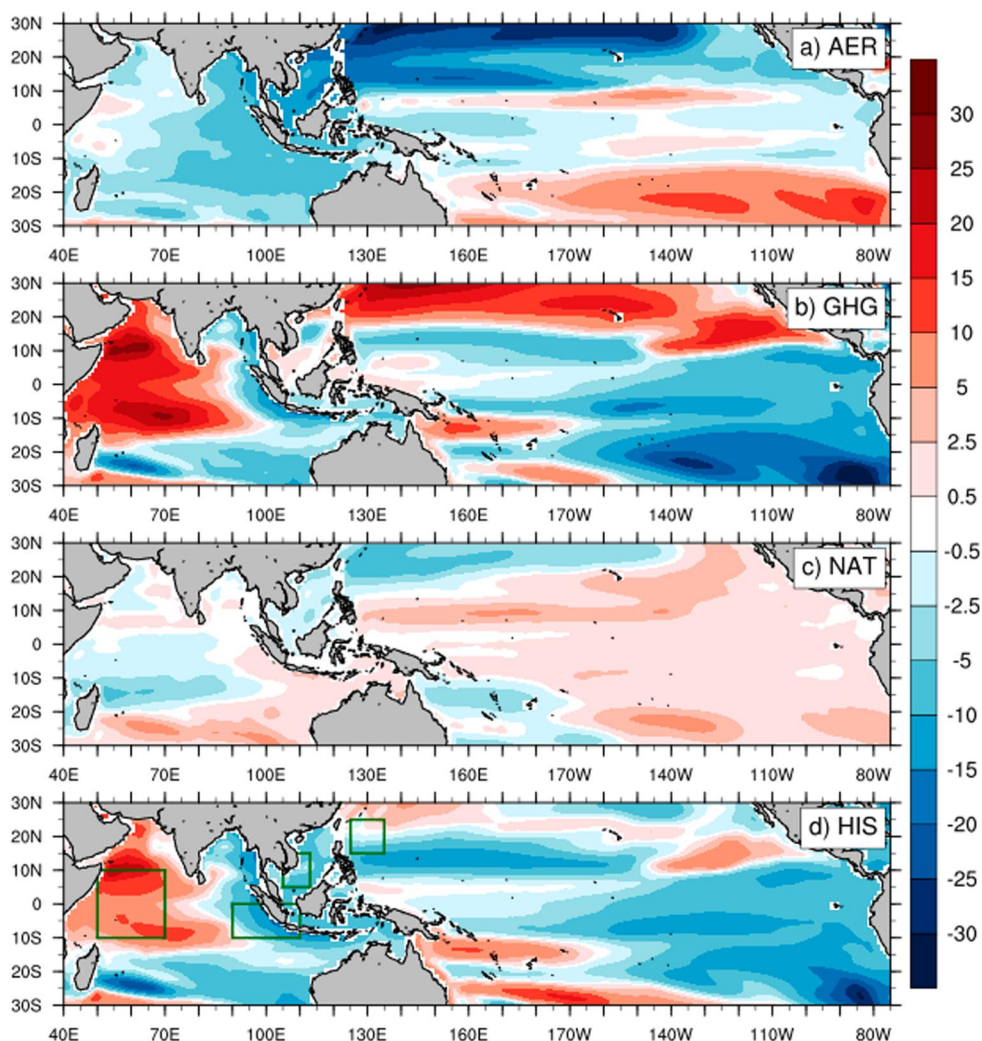


Figure 2. CanESM ensemble mean dynamic sea level (DSL) change (1985–2014 minus 1950–1979; in mm) for (a) aerosol only forcing (AER), (b) greenhouse gas only forcing (GHG), (c) natural only (NAT), and (d) historical forcing (HIS). Boxes marked in (d) indicate the regions of time series analysis shown in Figure 5.

models are shown in Supporting Information S1. Earlier literature addressed CanESM's capability to simulate sea level realistically (e.g., Ferrero et al., 2021). Furthermore, CanESM's DSL drift in the control simulation is substantially less than that of CNRM and IPSL (Figure S2 in Supporting Information S1). Nonetheless, all three models used here reproduce the mean (1993–2014) DSL reasonably well (Figure S3 in Supporting Information S1).

Here we also discuss the steric sea level, which can be estimated by combining the global thermosteric sea level and DSL. In other words, steric sea-level change is the sum of steric sea-level change and mass distribution change (Cha et al., 2023).

2.2. Quantification of Sea-Level Changes

We quantify the anthropogenic and natural forcings of steric and manometric sea-level changes. Steric sea-level change is related to the change in ocean density, assuming the local mass of the ocean per unit area remains constant (Gregory et al., 2019). Therefore, steric sea-level change is only associated with vertical expansion or contraction of the water column in response to local density change (Gregory et al., 2019; Landerer et al., 2007). Manometric sea level is a non-steric sea-level component due to changes in the local mass of the ocean per unit area, assuming constant density (Gregory et al., 2019). Manometric sea level can be estimated from the ocean

bottom water pressure. Our selected CMIP6 models do not include barostatic contributions from land sources. We quantify the steric sea-level changes by considering sea surface elevation ζ' as the sum of three terms (Griffies & Greatbatch, 2012):

$$\zeta' = \zeta_a + p'_b g^{-1} \rho_0^{-1} + \zeta'_s \quad (2)$$

where ζ_a is the inverted barometer effect to sea level, $p'_b g^{-1} \rho_0^{-1}$ is manometric sea level (i.e., the contribution from ocean bottom pressure changes; Gregory et al., 2019), and ζ'_s is the steric sea-level contribution. We use the CMIP6 variables *pbo*, *thetao*, and *so* for ocean bottom water pressure, temperature, and salinity, respectively. Steric sea-level changes are integrated from a depth of H (here the bottom of the ocean) to the free surface (i.e., $H = -H$ to $H = 0$). Here ρ_0 is referenced to seawater density at 0°C and 35 psu. Here ζ_a is zero, as surface pressure forcing is set to zero in Boussinesq models (Landerer et al., 2007; Yin et al., 2010), meaning DSL and steric sea-level changes are only equivalent if the manometric sea level is zero. As CMIP6 models do not include barostatic sources, all bottom pressure changes occur due to mass redistribution within the global ocean (Landerer et al., 2007). Here we assume that the steric sea level can be written as the following equation

$$\zeta'_s = \zeta_s^{\text{thermo}} + \zeta_s^{\text{halo}} \quad (3)$$

where ζ_s^{thermo} and ζ_s^{halo} are individual temperature and salinity contributions (Gregory et al., 2019), respectively, to the steric anomalies by following a similar approach of Yin et al. (2010). While not considered here, trends in evaporation, precipitation, and terrestrial water storage can also contribute to changes in ocean volume. The thermosteric (ζ_s^{thermo}) and halosteric (ζ_s^{halo}) sea-level changes are calculated using the annual mean CMIP6 data as:

$$\zeta_s^{\text{thermo}} = \frac{1}{\rho_0} \int_{-H}^0 [\rho(T, S_R, p_R) - \rho(T_R, S_R, p_R)] dz \quad (4)$$

$$\zeta_s^{\text{halo}} = \frac{1}{\rho_0} \int_{-H}^0 [\rho(T_R, S, p_R) - \rho(T_R, S_R, p_R)] dz \quad (5)$$

here T_R , S_R , p_R are temperature, salinity, and pressure for the reference state (1950–1979 average). Before performing the above calculations, we convert potential temperature and practical salinity to conservative temperature and absolute salinity using the Thermodynamic Equation of Seawater 2010 package (McDougall & Barker, 2011). Ocean density is a nonlinear function of temperature, salinity, and pressure, so this partitioning of density change is approximate (Yin et al., 2010). The steric sea-level change definition assumes no horizontal movement of mass. However, in reality, due to the presence of horizontal transports, it is almost impossible to separate density changes due to local changes in properties from those due to the movement of mass (Gregory et al., 2019). The consideration of fixed density in the above calculations, therefore, brings an additional approximation. We calculate thermosteric and halosteric sea level at each time step and then show the change between two periods after removing the weighted global mean of the corresponding forcing (i.e., AER, GHG, etc.). The area-weighted mean is calculated using the CMIP6 variable *areacello* which contains the area of each grid point. To compute the weighted mean, we multiply the steric sea level at each grid point by the area that the grid point represents and then divide the total area of global ocean points.

3. Results

3.1. Indo-Pacific Warm Pool Sea-Level Change

We first evaluate the evolution of global thermosteric changes relative to 1950. Historical simulations in all three models show that the global thermosteric sea level has risen up to 45 mm relative to 1950 (Figure S4 in Supporting Information S1). This rise is consistent with the observed global thermosteric sea-level trend of 0.71 mm/year from 1957 to 2018 (Frederikse et al., 2020). Our results show that the rise in global thermosteric sea level is primarily forced by the GHG. The GHG forcing run shows an increased thermosteric sea level of nearly 80 mm from 1950 to 2014. The AER-forced run acts in a compensatory manner, such that this increase is reduced when considering their joint effect in the historical simulation. Despite the spread in magnitudes of GHG and AER

forcing in these three models, they agree on the rapid rise of thermosteric sea-level patterns since 1970 (Figure S4 in Supporting Information S1).

We further examine DSL changes over the Indo-Pacific warm pool region for different forcings. The AER forcing causes an overall fall in DSL (Figure 2). Conversely, GHG forcing causes a DSL rise (Figure 2b). These DSL changes suggest that AER and GHG forcing are compensatory when averaged spatially over a domain (Figures 2a and 2b). Overall, the historical simulation (Figure 2d) shows a fall in DSL in the region, except over the western Indian Ocean, the eastern Australian coast, and around 20°N (nearly collocated with the North Equatorial Current), where DSL has risen in recent decades. Over the South China Sea, a historical DSL fall of up to 15 mm is noted (Figure 2d). In contrast, the western Indian Ocean shows a rise in DSL of up to 30 mm during a similar period (Figure 2d). The other two models (CNRM and IPSL) show similar changes in DSL patterns in recent decades (Figure S5 in Supporting Information S1). The linear trend analysis (based on the Mann-Kendall test) of DSL changes reveals a similar pattern of DSL changes in Figure 2 (Figures S5 and S6 in Supporting Information S1), with a GHG induced rising trend of up to 0.8 mm/year over the western Indian Ocean and up to 0.7 mm/year of a falling trend over the eastern Indian Ocean region. A weak negative DSL trend is also observed over the Southeast Asian seas, including the South China Sea. Meanwhile, the eastern Pacific shows a GHG-induced falling DSL trend in all three models. As these results are derived from individual forcing simulations, the DSL changes are very likely the response to specific forcings in the simulation. Despite the spatial diversity in the magnitude of DSL changes, the steric sea-level change indicates GHG forcing driven historical rise in the Indo-Pacific warm pool region (Figure 2, Figure S4 in Supporting Information S1).

3.2. Attribution of Indo-Pacific Warm Pool Sea-Level Change in Different Components

We estimate steric sea-level changes over the Indo-Pacific warm pool region in response to natural and anthropogenic forcings (Figure 3). We show the local thermosteric and halosteric sea-level changes after removing the global mean. In other words, Figure 3 shows the regional anomalies compared to the global mean. We focus on changes in spatial patterns and magnitude from different forcings while identifying the causes of historical sea-level changes. Thermosteric sea-level anomalies are reduced in the region due to AER forcing, except in the coastal and shallow regions of Southeast Asia and the north equatorial current region in the Pacific Ocean (Figure 3a). In contrast, GHG forcing shows an increase in thermosteric anomalies in the Indian Ocean and a decrease in the Pacific Ocean and Southeast Asia (Figure 3b). The compensatory impact of AER and GHG forcing in the region is evident, particularly in the shallow and coastal regions (Figure 3). Overall, the thermosteric anomalies in historical simulation (Figure 3d) are largely controlled by the pattern and magnitude of GHG forcing (Figure 3b). The maximum historical anomaly in the thermosteric component due to GHG forcing (Figure 3b) is noted over the western Indian Ocean and east of Australia, coinciding with the highest rise in the DSL (Figure 2b). The NAT forcing on the thermosteric sea level is relatively negligible in the region (Figure 3c). The differing thermosteric responses in the region reflect the formation of deep water and enhanced ventilation (Landerer et al., 2007), which helps the warming signal penetrate deeper layers in those layers, such as over the western Indian Ocean and the South China Sea.

Halosteric sea level is associated with regional salinity changes due to changes in local freshwater balance (e.g., precipitation, evaporation, river runoff) (Gregory et al., 2019). AER forcing drives negative anomalies in halosteric sea level in the northern tropical Pacific and Southeast Asian seas (Figure 3e), while other regions reflect positive anomalies. Historical simulation (Figure 3h) shows positive anomalies in halosteric components in the western Pacific Ocean and the western Indian Ocean (up to 60 mm) from GHG forcing. Similar to thermosteric anomalies, the NAT forcing induced halosteric anomalies are weaker in the region compared to GHG or AER forcing. Similar to the DSL pattern (Figures 2b and 2d) an IOD-like east-west gradient in the Indian Ocean is reflected in halosteric changes, which are mostly driven by GHG forcing. Notably, the regional thermosteric and halosteric sea-level anomalies are of opposite sign (relative to the global mean) over the northern and western Pacific Ocean. The historical rise in steric height over this region is predominantly the result of halosteric change (e.g., Durack et al., 2014).

We further investigate the manometric change from different forcings (Figure 4) that is often used for ocean warming detection (Landerer et al., 2007; Yin et al., 2010). A strong manometric sea-level rise up to 20 mm over the Indo-Pacific warm pool region is detected from AER forcing, except for the coastal regions and shallow oceans in Southeast Asia (Figure 4a, Figure S7 in Supporting Information S1). The GHG forcing reflects the

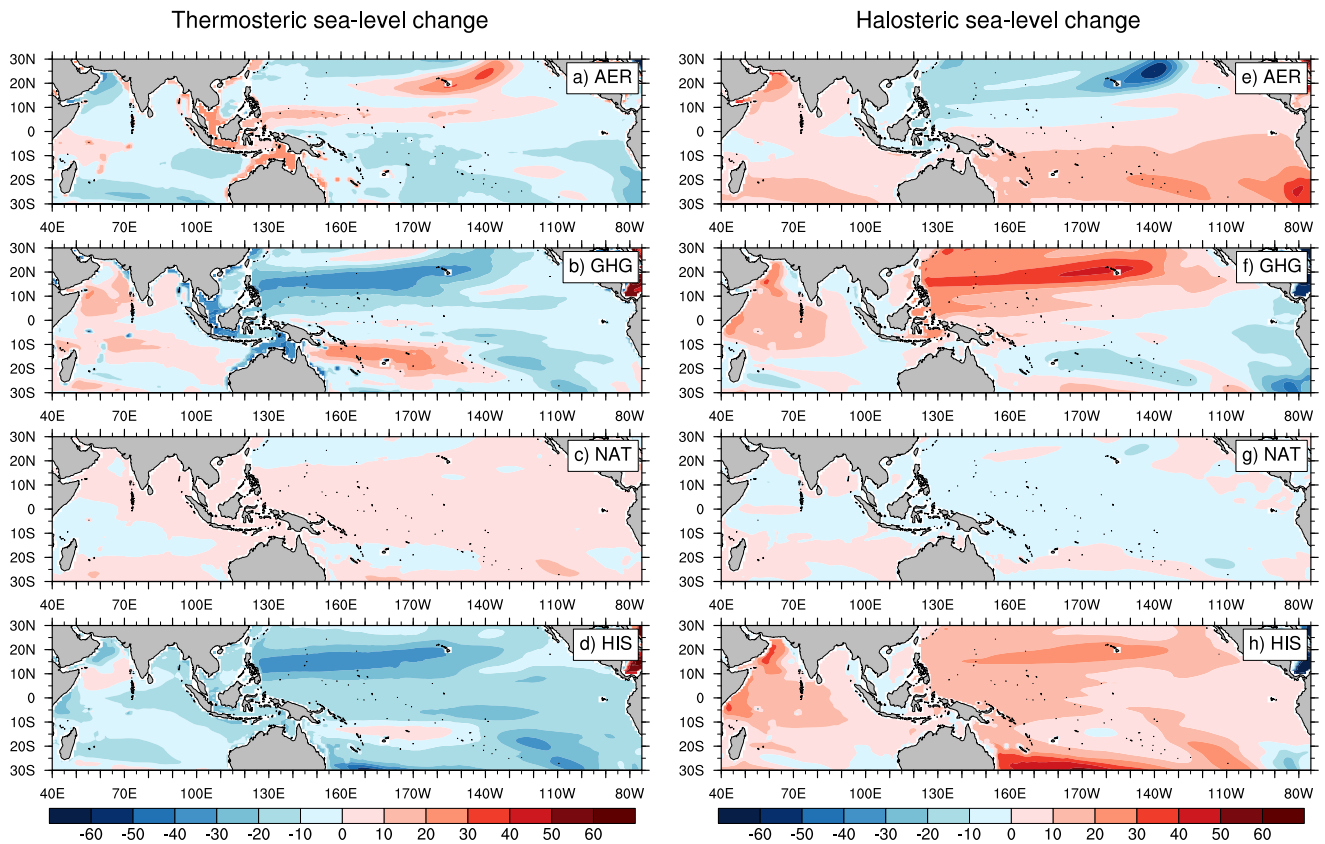


Figure 3. CaneSM ensemble mean steric sea-level change (1985–2014 minus 1950–1979; in mm): (a–d) thermosteric and (e–h) halosteric components. Thermosteric and halosteric sea-level changes are for aerosol-only (AER; a, e), greenhouse gas-only (GHG; b, f), natural only (NAT; c, g), and historical (HIS; d, h) simulations. The weighted global mean is removed for each forcing.

opposite sign but a similar pattern of manometric sea-level change in the region, with up to 50 mm of rise in the shallow and coastal regions (Figure 4b). The NAT forcing has an overall weak impact on manometric sea level (Figure 4c). Due to the strong but opposite impact of AER and GHG forcings, the historical simulations exhibit a ~ 5 mm manometric sea-level fall over deep oceans but up to a 20 mm rise over shallow oceans in Southeast Asia and coastal regions (Figure 4d). The manometric sea-level changes in shallow water are significantly higher than the steric sea-level changes (Figure 3). Conversely, the steric sea level in deep water oceans is higher than the manometric contribution (Gregory et al., 2019; Yin et al., 2010). The regions of deeper oceans absorb more heat in a warming climate (Fox-Kemper et al., 2021) compared to shallower oceans. As a result, the lack of balance between strong steric sea-level gradients across the shelves and geostrophy leads to a substantial manometric sea-level rise over shallow oceans (Figure 4; Landerer et al., 2007). The increased mass on continental shelves amplifies gravitational attraction and causes the sea floor to lower during additional loading, leading to sea-level rise on shallow shelves due to GHG forcing (Richter et al., 2013). Over the Indo-Pacific warm pool region, manometric sea-level change from NAT forcing (Figure 4c) is relatively less than anthropogenic forcing (Figures 4a and 4b). This rise in NAT-induced manometric sea level over tropical and subtropical oceans (away from shallow shelves) is likely balanced by a NAT-induced fall over polar regions (Richter et al., 2013).

3.3. Time of Emergence

We explore the evolution of the anthropogenic component of DSL change and some physical drivers in different regions of the Indo-Pacific warm pool. We focus on four key regions where DSL has changed significantly over the historical period (Figure 2d). Here, using the concept of *time of emergence* (Walker et al., 2022), we indicate when a single anthropogenic forcing drives the signal beyond the spread of variability from the NAT simulation. By following this approach, we find historical DSL changes by 2014 in the Indo-Pacific warm pool region are well beyond the ensemble spread of DSL changes in the NAT simulation (Figure 5, Figure S8 in Supporting

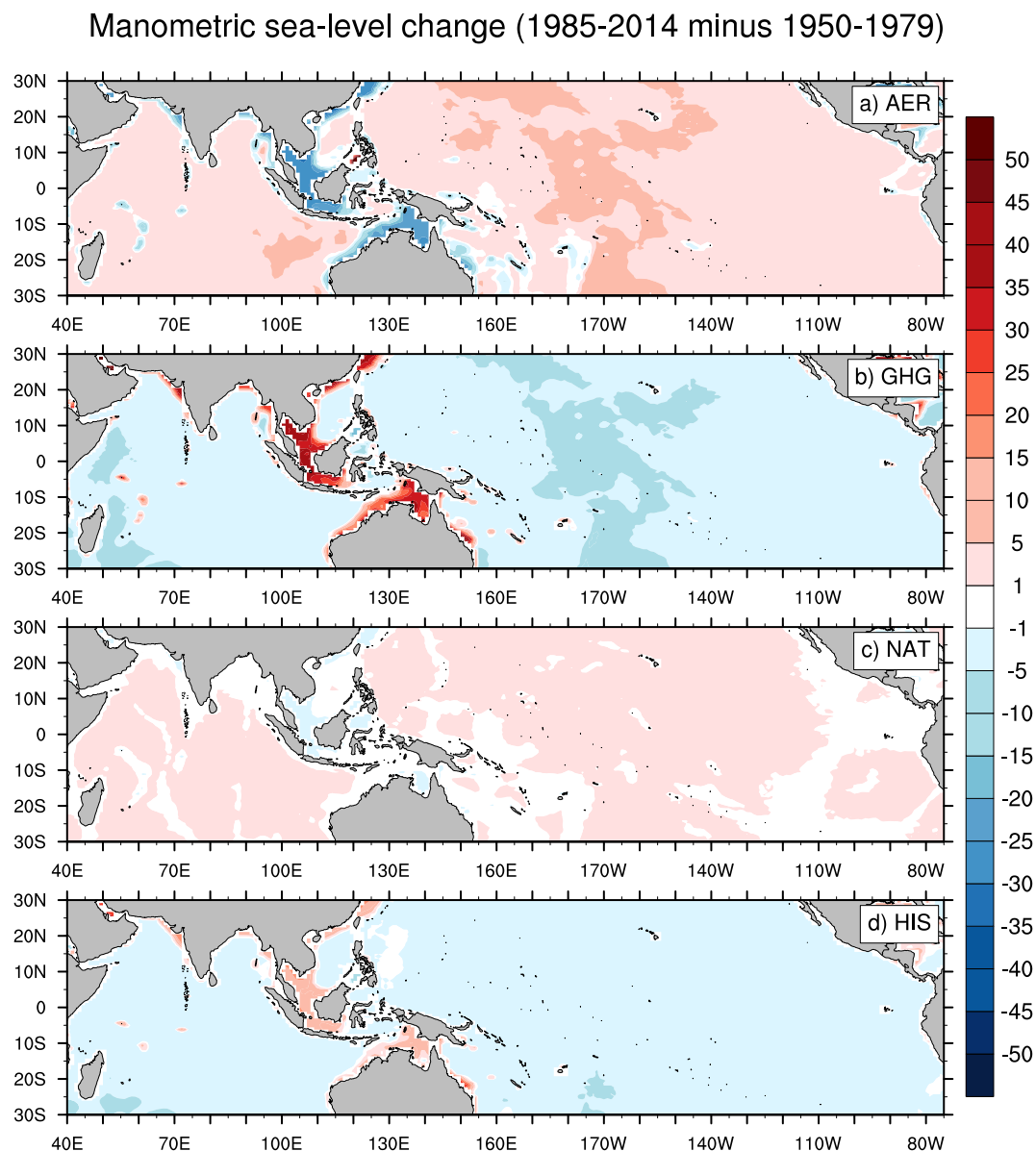


Figure 4. CanESM ensemble mean manometric sea-level change (1985–2014 minus 1950–1979; in mm) for (a) aerosol-only (AER), (b) greenhouse gas-only (GHG), (c) natural-only (NAT), and (d) historical (HIS) simulations.

Information S1). DSL has risen over the western Indian Ocean (~35 mm; Figure 5a) and western Pacific Ocean (~15 mm; Figure S8b in Supporting Information S1) by the end of 2014 relative to 1850. While, over the same period, DSL has fallen over the eastern Indian Ocean (~20 mm; Figure 5b) and the South China Sea (~10 mm; Figure S8a in Supporting Information S1). In general, DSL rise is associated with sea-level pressure fall and weaker zonal wind speed (westerlies) and vice versa in the region. However, this association of DSL and zonal wind speed (westerlies) in the South China Sea (Figure S8a in Supporting Information S1) is not clear due to its location and the possible role of meridional wind related to monsoons (e.g., Shaw & Chao, 1994). The time series analysis (Figure 5, Figure S8 in Supporting Information S1) demonstrates: (a) the time of emergence of the anthropogenic signal varies regionally, indicating the role of regional-local scale climate dynamics; and (b) the total anthropogenic impact on DSL (and other variables) is significantly reduced by the AER, indicating historical DSL changes are driven by the balance between GHG and AER forcings. Overall, we note that anthropogenic signals in DSL within the Indo-Pacific warm pool region emerged first in the western Indian Ocean around 1940 (Figure 5a) and last in the eastern Indian Ocean around 1970. In contrast, the western Pacific region shows a

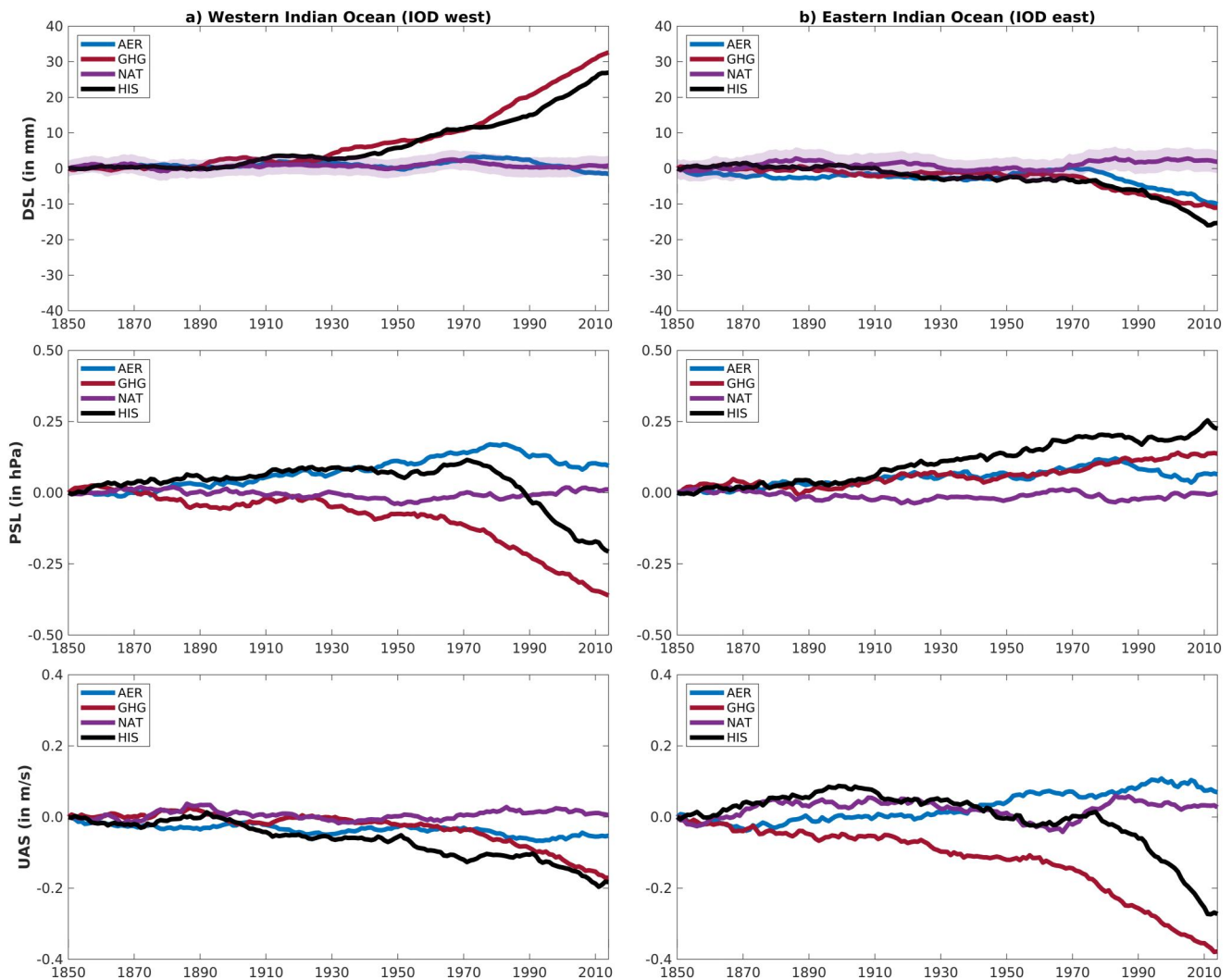


Figure 5. CaneSM ensemble mean time series of relative change (w.r.t. 1850 average) of (top panel) dynamic sea level (DSL, in mm), (mid-panel) sea-level pressure (PSL, in hPa) and (bottom panel) near-surface zonal wind speed (UAS, in m; positive eastward) averaged over (a) western Indian Ocean (Indian Ocean Dipole [IOD] west), and (b) Eastern Indian Ocean (IOD east). Smoothed (by 20 years moving mean) time series are averaged over (a) western Indian Ocean (10°S – 10°N , 50°E – 70°E), (b) eastern Indian Ocean (10°S –EQ, 90°E – 110°E). Different forcings are indicated in different colors and the legend. AER = aerosol-only; GHG = greenhouse gas-only; NAT = natural-only; HIS = historical. The shaded region in the top panel (a–b) indicates uncertainty (1 standard deviation) in DSL changes from NAT forcing.

higher spread of NAT forcing, which is consistent with the substantial role of low-frequency natural climate variability in the region (e.g., Hamlington, Strassburg, et al., 2014). The time of emergence of anthropogenic sea-level signals from atmospheric forcing may depend on chaotic ocean variability that varies from basin to basin (e.g., Llovel et al., 2018). The smaller spread within ensembles of the historical DSL signal (Figure S9 in Supporting Information S1) lends additional confidence in the results.

4. Discussion

4.1. Physical Drivers for Indo-Pacific Sea-Level Changes

We show regional diversity in historical DSL changes, with rise in the western Indian Ocean but fall over the South China Sea and the eastern Indian Ocean (Figure 2). This regional variability of historical DSL may be due to a variety of physical drivers. For example, Dittus et al. (2021) argued that anomalous Rossby wave train induced higher sea-level pressure and cooling over the northern Pacific Ocean can be a consequence of anthropogenic AER forcing. The historical DSL rise in the western Indian Ocean may be a consequence of unusual western Indian Ocean warming relative to the entire tropical Indo-Pacific region (Roxy et al., 2014). A

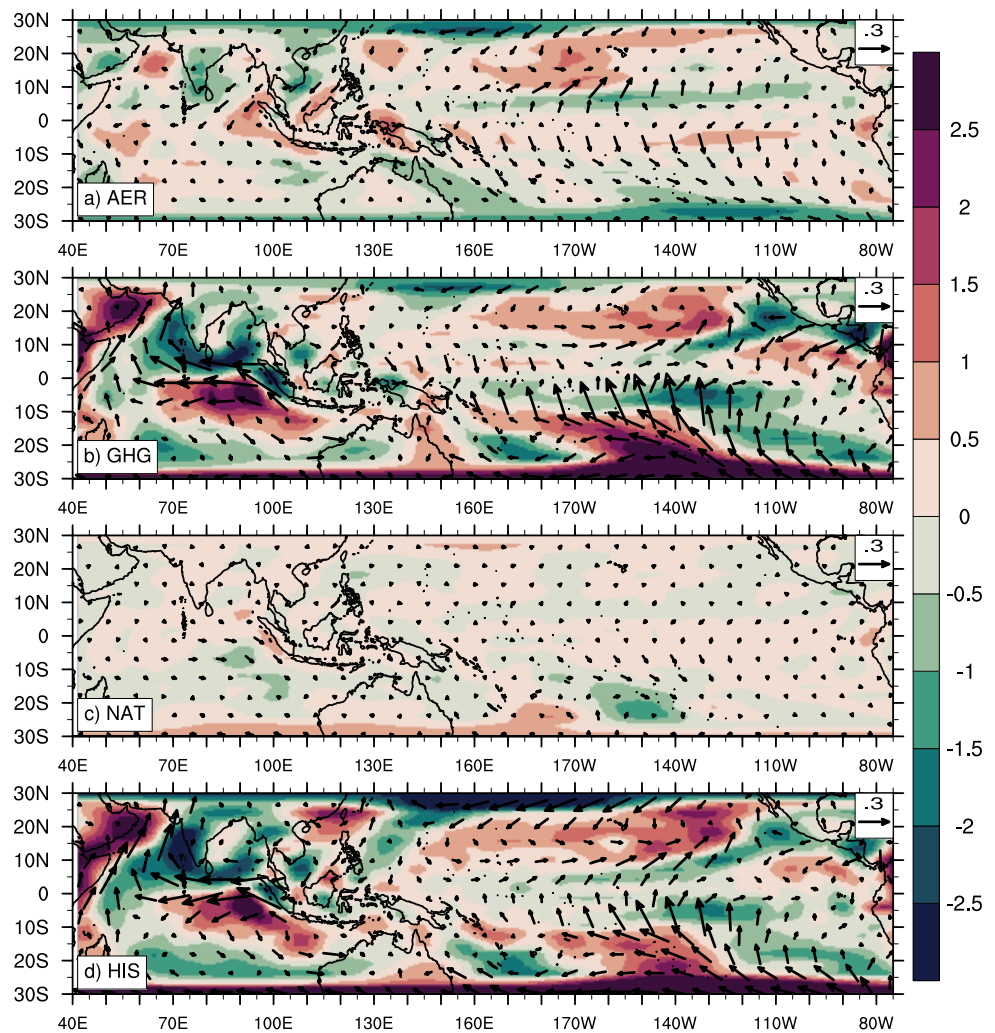


Figure 6. CanESM ensemble mean change (1985–2014 minus 1950–1979) in near-surface wind pattern (vectors; in m/s) and wind stress curl (shaded; in 10^{-7} N/m³). Wind pattern changes for (a) aerosol only (AER), (b) greenhouse gas only (GHG), (c) natural only (NAT), and (d) historical (HIS) simulations.

positive IOD-like pattern in historical DSL changes is evident in the Indian Ocean, probably linked to the increased occurrence of intense positive IOD events in recent decades attributed to GHG warming (Cai et al., 2021). The zonal gradient of the DSL change in the tropical Pacific Ocean (Figure 2, Figure S5 in Supporting Information S1) appears to be a coupled response with the Walker circulation. While a consistent pattern of DSL changes and trends demonstrates the robustness of the results, the diverse magnitudes across the models reveal the varying sensitivities of the CMIP6 models to anthropogenic AER forcing (Ushijima et al., 2022).

We study the near-surface wind pattern changes to examine the physical drivers for the DSL changes (Figure 6, Figure S10 in Supporting Information S1). The GHG-induced stronger easterly wind anomaly over the eastern Indian Ocean causes a positive IOD-like pattern in the tropical Indian Ocean. Over the South China Sea, the historical wind pattern changes are not pronounced, whereas weak westerlies in the central to eastern Pacific are evident. Surface wind patterns over the warm pool region changed due to AER and NAT forcing being much weaker relative to GHG forcing. The zonal wind speed arising from AER forcing is easterly over the warm pool region, whereas it is weaker westerly from NAT forcing. The results suggest that the historical changes in the near-surface wind pattern (Figure 6d, Figure S10d in Supporting Information S1) in the study region are dominated by GHG forcing (Figure 6b, Figure S10b in Supporting Information S1). Here, the wind patterns are somewhat smooth because of the ensemble mean, and showing the difference between the 30 years mean period.

Many of the changes in DSL are associated with changes in wind stress curl (Figure 6). For example, negative wind stress curl over the western Indian Ocean and positive over the eastern equatorial Pacific and north of the equator (Figure 6) are associated with rise and fall in DSL (Figure 2), respectively. The wind stress curl affects sea level by imposing changes in Ekman transport. The negative wind stress curl creates a convergence of water and causes the local sea level to rise in the northern hemisphere. This relationship is opposite in the southern hemisphere (Sueyoshi & Yasuda, 2012; Timmermann et al., 2010). Moreover, wind stress curl changes trigger westward-propagating oceanic Rossby waves that are associated with sea-level anomalies along their propagation pathways (Timmermann et al., 2010). Thus, wind-induced changes in the tropical Indo-Pacific warm pool region strongly contribute to the regional characteristics of sea-level changes.

Atmospheric pressure changes at sea level are generally anti-correlated with DSL changes (Figure 5, Figure S8 in Supporting Information S1). However, this relationship is not independent of location (Ponte, 1994). For example, we find the correlation between DSL and sea-level pressure in the western Pacific Ocean to be weak, and therefore, DSL changes under different natural and anthropogenic forcings cannot be readily explained via sea-level pressure changes (Figure 5, Figure S8 in Supporting Information S1). Due to the complexity and role of multiple physical processes, sea-level changes cannot always be attributed to a subset of mechanisms (Piecuch & Ponte, 2011), such as only by wind patterns or sea-level pressure changes. Understanding sea-level changes in the Indo-Pacific warm pool region is complex due to the interactions among complex processes that are associated with natural climate variabilities across different timescales (Cazenave & Nerem, 2004; Hamlington et al., 2020, 2021; Hamlington, Strassburg, et al., 2014; Han et al., 2019).

Manometric sea level is commonly overlooked in sea-level studies (Landerer et al., 2007), particularly for regional sea-level attribution. We show that local change in mass is an important driver of sea-level rise in shallow and coastal regions (Figure 4, Figure S7 in Supporting Information S1). This increase in mass in shallow regions appears to be indirectly driven by increased GHG forcings (Figure 4). We find the maximum historical manometric sea-level rise is up to 15 mm, compared to the maximum of 30 mm DSL changes in the Indo-Pacific region (Figures 2 and 4). Richter et al. (2013) showed that the impact of shelf mass loading due to ocean bottom water pressure can increase sea-level rise by up to 10% of the total sea level in the Indo-Pacific warm pool region. Nonetheless, ocean bottom pressure is used as a static load, implying that the resulting self-attraction and loaded effects will determine the equilibrium ocean configuration, but they are not coupled to the CMIP6 models used here. It should be noted that Boussinesq models do not feel the effects of atmospheric pressure changes directly, but are affected indirectly through changes in wind stress.

While we are motivated here by long-term regional sea-level changes, the role of Madden-Julian Oscillation on an intraseasonal timescale (Oliver & Thompson, 2010; Vialard et al., 2009; X. Zhang et al., 2009), monsoon on seasonal and semi-annual timescales (e.g., McCreary et al., 1996; Qu et al., 2022), IOD and El Niño Southern Oscillation on an interannual timescale (e.g., Hameed et al., 2018; McPhaden et al., 2006), and Pacific Decadal Oscillation on a decadal timescale (Deepa et al., 2021; Nidheesh et al., 2019; Piecuch et al., 2019) and even remote oceanic Rossby and Kelvin wave forcing (e.g., Cheng et al., 2016) may be important for sea-level attribution and demand further investigation. Although we argue the positive IOD-like change in the tropical Indian Ocean in the climate change time scale (shown as the difference between two 30 years period), the impact of different natural and anthropogenic forcings on IOD characteristics on the interannual scale is beyond the scope of this work.

4.2. Limitations of the Present Study

One of the major caveats of CMIP6-based attribution studies is the absence of barystatic components in the model simulations. An improved representation of physical processes important for the polar climate in CMIP6 models may reduce uncertainty in sea-level simulations (Li et al., 2023; J. Y. Park et al., 2023; Topál et al., 2022). We also recognize that global climate models have several mean-state biases over the Indo-Pacific region (e.g., I. H. Park et al., 2022; Samanta, Hameed, et al., 2018; Samanta, Karnauskas, et al., 2018, 2019; Wills et al., 2022) including in CanESM (Swart et al., 2019), which may impact sea-level simulation but are not investigated here. For example, Lyu et al. (2020) argued that the DSL rise in the western tropical Pacific Ocean is underestimated in CMIP6 models due to the cold-tongue SST bias in the tropical Pacific. In addition, the role of changing ocean transport in Southeast Asian seas (Samanta et al., 2021), climate shift (Kannad et al., 2022), interbasin interaction (Hameed et al., 2018; L. Zhang et al., 2019), multiscale interactions among climate variabilities (Han et al., 2017), and even land subsidence (Tay et al., 2022) on sea-level changes over the Indo-Pacific warm pool region may be

important. One of the limitations of DAMIP simulations is their coarse horizontal resolution (~ 100 km; Table S2 in Supporting Information S1) than is optimal for local-scale studies. An increase in horizontal resolution in future DAMIP simulations or coordinated efforts on regional coupled downscaling experiments of DAMIP simulations may provide finer details of sea-level changes in response to various anthropogenic and natural forcings. Quantifying the impact of these factors on sea-level attribution is not an easy task due to its complexity, which involves multiple processes and therefore requires further research.

5. Summary

Despite a substantial number of global-scale studies (e.g., Jevrejeva et al., 2009; Slangen et al., 2014, 2016), attributing anthropogenic signals to sea-level changes at the regional-local scale is limited and remains challenging (e.g., Hamlington et al., 2020; Richter et al., 2020). The existing regional or basin average studies (e.g., Marcos et al., 2017) provide an important background for anthropogenic sea-level change, yet the spatial patterns of such changes are important and demand better understanding. We attribute spatiotemporal patterns of sea-level changes using large ensemble (varying from 10 to 30) simulations of DAMIP/CMIP6 climate models. We focus on the Indo-Pacific warm pool region due to its rapid expansion (Figure 1c) from anthropogenic factors (Weller et al., 2016), rapid sea-level rise, and the presence of densely populated low-income coastal regions (Figure 1a). In addition to global thermosteric sea-level, we show patterns and magnitudes of regional changes in DSL, steric, and manometric contributions in recent decades. Our results indicate the dominance of GHG induced changes in the historical period; however, diversity in the emergence of such an anthropogenic signal on a spatiotemporal scale persists. We particularly highlight the positive IOD-like sea-level changes in the Indian Ocean in DSL and halosteric changes. Furthermore, we show the important contribution of the manometric component to sea-level rise over shallow oceans and coastal regions of the Indo-Pacific warm pool region with increasing GHG concentrations.

Our finding is consistent with earlier detection and attribution studies that demonstrate the offsetting role of anthropogenic AER in GHG forcing on global warming (e.g., Gillett et al., 2013, 2021). Nevertheless, the detailed study of the regional pattern of these responses on sea-level changes had not been undertaken previously. Southeast Asia's sea level and ocean dynamics are affected by both the tropical Pacific and Indian Oceans (e.g., Samanta et al., 2021). Our results indicate a GHG-induced positive IOD-like pattern in sea-level change, likely due to the increased frequency of extreme IOD events (e.g., Cai et al., 2014). Zheng et al. (2013) reported a shoaling thermocline in the eastern Indian Ocean in response to GHG warming, which can lead to positive IOD-like mean state changes. DiNezio et al. (2020) argued for a similar emergence of the Indian Ocean mode in response to GHG forcing over the equatorial region. These basin-wide changes in the Indian Ocean can also impact Southeast Asia's sea level.

When making regional coastal management and adaptation decisions, we must understand the regional-to-local scale difference in sea level in response to anthropogenic forcing. For example, enhanced anthropogenic sea-level rise in the Indo-Pacific warm pool region exacerbates tropical cyclone and flood impacts in a warming climate (Fasullo & Nerem, 2018). Our results provide fresh insights into the substantial human influence on regional-to-local scale sea-level change over the Indo-Pacific warm pool region to date, and the urgency of adaptation and mitigation actions needed to ensure a sustainable future.

Conflict of Interest

The authors declare no conflicts of interest relevant to this study.

Data Availability Statement

Sea-level data used in Figure 1 is available from Copernicus Climate Change Service, Climate Data Store (2018).

Gridded population data is available from Warszawski et al. (2017). GeoTIFF files were converted to NetCDF using Geospatial Data Abstraction Library (GDAL) available from <https://gdal.org/>.

Observational SST data (HadISST1) is available from Rayner et al. (2003).

DAMIP/CMIP6 model data is available from <https://esgf-node.llnl.gov/search/cmip6/>.

Thermodynamic Equation of Seawater 2010 (TEOS-10) is available from McDougall and Barker (2011).

Acknowledgments

DS acknowledges Justin Dauwels and Benjamin Grandey for useful discussions. We acknowledge the World Climate Research Programme, which, through its Working Group on Coupled Modeling, coordinated and promoted CMIP6. We thank the climate modeling groups for producing and making available their model output, the Earth System Grid Federation (ESGF) for archiving the data and providing access, and the multiple funding agencies that support CMIP6 and ESGF. Figures were created using Matlab 2022b and NCAR Command Language (version 6.6.2) [Software]. (2019). Boulder, Colorado: UCAR/NCAR/CISL/TDD. <https://doi.org/10.5065/D6WD3XH5>. This Research is supported by the National Research Foundation, Singapore, and National Environment Agency, Singapore under the National Sea level Programme Funding Initiative (Award No. USS-IF-2020-3). Any opinions, findings, conclusions, or recommendations expressed in this material are those of the author(s) and do not reflect the views of the National Research Foundation, Singapore, and the National Environment Agency, Singapore. This study was also supported by Singapore Ministry of Education (MOE) Academic Research Fund Tier 3 Project MOE-2019-T3-1-004 funded at Earth Observatory of Singapore. This is Earth Observatory of Singapore contribution number 520. KBK acknowledges funding support from the NASA Sea level Change Science Program, Award 80NSSC20K1123.

References

- Bai, W., Liu, H., Lin, P., Hu, S., & Wang, F. (2022). Indo-Pacific warm pool present warming attribution and future projection constraint. *Environmental Research Letters*, *17*(5), 054026. <https://doi.org/10.1088/1748-9326/ac5edf>
- Bonnet, R., Boucher, O., Deshayes, J., Gastineau, G., Hourdin, F., Mignot, J., et al. (2021). Presentation and evaluation of the IPSL-CM6A-LR Ensemble of extended historical simulations. *Journal of Advances in Modeling Earth Systems*, *13*(9), e2021MS002565. <https://doi.org/10.1029/2021ms002565>
- Boucher, O., Servonnat, J., Albricht, A. L., Aumont, O., Balkanski, Y., Bastrikov, V., et al. (2020). Presentation and evaluation of the IPSL-CM6A-LR climate model. *Journal of Advances in Modeling Earth Systems*, *12*(7), e2019MS002010. <https://doi.org/10.1029/2019ms002010>
- Cai, W., Santoso, A., Wang, G., Weller, E., Wu, L., Ashok, K., et al. (2014). Increased frequency of extreme Indian Ocean Dipole events due to greenhouse warming. *Nature*, *510*(7504), 254–258. <https://doi.org/10.1038/nature13327>
- Cai, W., Yang, K., Wu, L., Huang, G., Santoso, A., Ng, B., et al. (2021). Opposite response of strong and moderate positive Indian Ocean Dipole to global warming. *Nature Climate Change*, *11*(1), 27–32. <https://doi.org/10.1038/s41558-020-00943-1>
- Cazenave, A., & Nerem, R. S. (2004). Present-day sea-level change: Observations and causes. *Reviews of Geophysics*, *42*(3), RG3001. <https://doi.org/10.1029/2003rg000139>
- Cha, H., Moon, J. H., Kim, T., & Song, Y. T. (2023). A process-based assessment of the sea-level rise in the northwestern Pacific marginal seas. *Communications Earth & Environment*, *4*(1), 300. <https://doi.org/10.1038/s43247-023-00965-5>
- Chen, H., He, Z., Xie, Q., & Zhuang, W. (2023). Performance of CMIP6 models in simulating the dynamic sea-level: Mean and interannual variance. *Atmospheric and Oceanic Science Letters*, *16*(1), 100288. <https://doi.org/10.1016/j.aosl.2022.100288>
- Cheng, X., Xie, S. P., Du, Y., Wang, J., Chen, X., & Wang, J. (2016). Interannual-to-decadal variability and trends of sea-level in the South China Sea. *Climate Dynamics*, *46*(9–10), 3113–3126. <https://doi.org/10.1007/s00382-015-2756-1>
- Copernicus Climate Change Service, Climate Data Store. (2018). *Sea-level gridded data from satellite observations for the global ocean from 1993 to present*. Copernicus Climate Change Service (C3S) Climate Data Store (CDS). <https://doi.org/10.24381/cds.4c328c78>
- Dangendorf, S., Marcos, M., Müller, A., Zorita, E., Riva, R., Berk, K., & Jensen, J. (2015). Detecting anthropogenic footprints in sea-level rise. *Nature Communications*, *6*(1), 1–9. <https://doi.org/10.1038/ncomms8849>
- De Deckker, P. (2016). The Indo-Pacific Warm Pool: Critical to world oceanography and world climate. *Geoscience Letters*, *3*(1), 1–12. <https://doi.org/10.1186/s40562-016-0054-3>
- Deepa, J. S., Gnanaseelan, C., & Parekh, A. (2021). The sea-level variability and its projections over the Indo-Pacific Ocean in CMIP5 models. *Climate Dynamics*, *57*(1–2), 173–193. <https://doi.org/10.1007/s00382-021-05701-3>
- DiNezio, P. N., Puy, M., Thirumalai, K., Jin, F. F., & Tierney, J. E. (2020). Emergence of an equatorial mode of climate variability in the Indian Ocean. *Science Advances*, *6*(19), eaay7684. <https://doi.org/10.1126/sciadv.aay7684>
- Dittus, A. J., Hawkins, E., Robson, J. I., Smith, D. M., & Wilcox, L. J. (2021). Drivers of recent North Pacific Decadal Variability: The role of aerosol forcing. *Earth's Future*, *9*(12), e2021EF002249. <https://doi.org/10.1029/2021ef002249>
- Dong, S., Sun, Y., Li, C., Zhang, X., Min, S. K., & Kim, Y. H. (2021). Attribution of extreme precipitation with updated observations and CMIP6 simulations. *Journal of Climate*, *34*(3), 871–881. <https://doi.org/10.1175/jcli-d-19-1017.1>
- Durack, P. J., Wijffels, S. E., & Gleckler, P. J. (2014). Long-term sea-level change revisited: The role of salinity. *Environmental Research Letters*, *9*(11), 114017. <https://doi.org/10.1088/1748-9326/9/11/114017>
- Eyring, V., Bony, S., Meehl, G. A., Senior, C. A., Stevens, B., Stouffer, R. J., & Taylor, K. E. (2016). Overview of the Coupled Model Inter-comparison Project Phase 6 (CMIP6) experimental design and organization. *Geoscientific Model Development*, *9*(5), 1937–1958. <https://doi.org/10.5194/gmd-9-1937-2016>
- Fasullo, J. T., & Nerem, R. S. (2018). Altimeter-era emergence of the patterns of forced sea-level rise in climate models and implications for the future. *Proceedings of the National Academy of Sciences*, *115*(51), 12944–12949. <https://doi.org/10.1073/pnas.1813233115>
- Ferrero, B., Tonelli, M., Marcello, F., & Wainer, I. (2021). Long-term regional dynamic sea-level changes from CMIP6 projections. *Advances in Atmospheric Sciences*, *38*(2), 157–167. <https://doi.org/10.1007/s00376-020-0178-4>
- Fox-Kemper, B., Hewitt, H. T., Xiao, C., Aðalgeirsdóttir, G., Drijfhout, S. S., Edwards, T. L., et al. (2021). Ocean, cryosphere and sea-level change.
- Frankignoul, C., Gastineau, G., & Kwon, Y. O. (2017). Estimation of the SST response to anthropogenic and external forcing and its impact on the Atlantic multidecadal oscillation and the Pacific decadal oscillation. *Journal of Climate*, *30*(24), 9871–9895.
- Frederikse, T., Landerer, F., Caron, L., Adhikari, S., Parkes, D., Humphrey, V. W., et al. (2020). The causes of sea-level rise since 1900. *Nature*, *584*(7821), 393–397. <https://doi.org/10.1038/s41586-020-2591-3>
- Gillett, N. P., Fyfe, J. C., & Parker, D. E. (2013). Attribution of observed sea-level pressure trends to greenhouse gas, aerosol, and ozone changes. *Geophysical Research Letters*, *40*(10), 2302–2306. <https://doi.org/10.1002/grl.50500>
- Gillett, N. P., Kirchmeier-Young, M., Ribes, A., Shiogama, H., Hegerl, G. C., Knutti, R., et al. (2021). Constraining human contributions to observed warming since the pre-industrial period. *Nature Climate Change*, *11*(3), 207–212. <https://doi.org/10.1038/s41558-020-00965-9>
- Gillett, N. P., Shiogama, H., Funke, B., Hegerl, G., Knutti, R., Matthes, K., et al. (2016). The detection and attribution model intercomparison project (DAMIP v1.0) contribution to CMIP6. *Geoscientific Model Development*, *9*(10), 3685–3697. <https://doi.org/10.5194/gmd-9-3685-2016>
- Goodkin, N. F., Samanta, D., Bolton, A., Ong, M. R., Hoang, P. K., Vo, S. T., et al. (2021). Natural and anthropogenic forcing of multi-decadal to centennial scale variability of sea surface temperature in the South China Sea. *Paleoceanography and Paleoclimatology*, *36*(10), e2021PA004233. <https://doi.org/10.1029/2021pa004233>
- Gregory, J. M., Griffies, S. M., Hughes, C. W., Lowe, J. A., Church, J. A., Fukumori, I., et al. (2019). Concepts and terminology for sea-level: Mean, variability and change, both local and global. *Surveys in Geophysics*, *40*(6), 1251–1289. <https://doi.org/10.1007/s10712-019-09525-z>
- Griffies, S. M., & Greatbatch, R. J. (2012). Physical processes that impact the evolution of global mean sea-level in ocean climate models. *Ocean Modelling*, *51*, 37–72. <https://doi.org/10.1016/j.ocemod.2012.04.003>
- Hameed, S. N. (2018). The Indian Ocean Dipole. In *Oxford research encyclopedia of climate science*.
- Hameed, S. N., Jin, D., & Thilakan, V. (2018). A model for super El Niños. *Nature Communications*, *9*(1), 1–15. <https://doi.org/10.1038/s41467-018-04803-7>
- Hamlington, B. D., Frederikse, T., Thompson, P. R., Willis, J. K., Nerem, R. S., & Fasullo, J. T. (2021). Past, present, and future Pacific sea-level change. *Earth's Future*, *9*(4), e2020EF001839. <https://doi.org/10.1029/2020ef001839>
- Hamlington, B. D., Gardner, A. S., Ivins, E., Lenaerts, J. T., Reager, J. T., Trossman, D. S., et al. (2020). Understanding of contemporary regional sea-level change and the implications for the future. *Reviews of Geophysics*, *58*(3), e2019RG000672. <https://doi.org/10.1029/2019rg000672>
- Hamlington, B. D., Leben, R. R., Strassburg, M. W., & Kim, K. Y. (2014). Cyclostationary empirical orthogonal function sea-level reconstruction. *Geoscience Data Journal*, *1*(1), 13–19. <https://doi.org/10.1002/gdj3.6>

- Hamlington, B. D., Strassburg, M. W., Leben, R. R., Han, W., Nerem, R. S., & Kim, K. Y. (2014). Uncovering an anthropogenic sea-level rise signal in the Pacific Ocean. *Nature Climate Change*, 4(9), 782–785. <https://doi.org/10.1038/nclimate2307>
- Han, W., Meehl, G. A., Stammer, D., Hu, A., Hamlington, B., Kenigson, J., et al. (2017). Spatial patterns of sea-level variability associated with natural internal climate modes. In *Integrative study of the mean sea-level and its components* (pp. 221–254).
- Han, W., Stammer, D., Thompson, P., Ezer, T., Palanisamy, H., Zhang, X., et al. (2019). Impacts of basin-scale climate modes on coastal sea-level: A review. *Surveys in Geophysics*, 40(6), 1493–1541. <https://doi.org/10.1007/s10712-019-09562-8>
- Hegerl, G., & Zwiers, F. (2011). Use of models in detection and attribution of climate change. *Wiley Interdisciplinary Reviews: Climate Change*, 2(4), 570–591. <https://doi.org/10.1002/wcc.121>
- Horton, B. P., Kopp, R. E., Garner, A. J., Hay, C. C., Khan, N. S., Roy, K., & Shaw, T. A. (2018). Mapping sea-level change in time, space, and probability. *Annual Review of Environment and Resources*, 43(1), 481–521. <https://doi.org/10.1146/annurev-environ-102017-025826>
- Jevrejeva, S., Grinsted, A., & Moore, J. C. (2009). Anthropogenic forcing dominates sea-level rise since 1850. *Geophysical Research Letters*, 36(20), L20706. <https://doi.org/10.1029/2009gl040216>
- Kannad, A., Goodkin, N. F., Samanta, D., Murty, S. A., Ramos, R. D., Smerdon, J. E., & Gordon, A. L. (2022). Drivers of coral reconstructed salinity in the South China Sea and Maritime Continent: The influence of the 1976 Indo-Pacific climate shift. *Journal of Geophysical Research: Oceans*, 127(6), e2021JC017787. <https://doi.org/10.1029/2021jc017787>
- Kopp, R. E., Hay, C. C., Little, C. M., & Mitrovica, J. X. (2015). Geographic variability of sea-level change. *Current Climate Change Reports*, 1(3), 192–204. <https://doi.org/10.1007/s40641-015-0015-5>
- Landerer, F. W., Jungclauss, J. H., & Marotzke, J. (2007). Regional dynamic and steric sea-level change in response to the IPCC-A1B scenario. *Journal of Physical Oceanography*, 37(2), 296–312. <https://doi.org/10.1175/jpo3013.1>
- Li, D., DeConto, R. M., & Pollard, D. (2023). Climate model differences contribute deep uncertainty in future Antarctic ice loss. *Science Advances*, 9(7), eadd7082. <https://doi.org/10.1126/sciadv.add7082>
- Llovel, W., Penduff, T., Meyssignac, B., Molines, J. M., Terray, L., Bessières, L., & Barnier, B. (2018). Contributions of atmospheric forcing and chaotic ocean variability to regional sea-level trends over 1993–2015. *Geophysical Research Letters*, 45(24), 13–405. <https://doi.org/10.1029/2018gl080838>
- Lyu, K., Zhang, X., & Church, J. A. (2020). Regional dynamic sea level simulated in the CMIP5 and CMIP6 models: Mean biases, future projections, and their linkages. *Journal of Climate*, 33(15), 6377–6398. <https://doi.org/10.1175/JCLI-D-19-1029.1>
- Maher, N., Milinski, S., Suarez-Gutierrez, L., Botzet, M., Dobrynin, M., Kornbluh, L., et al. (2019). The Max Planck Institute Grand Ensemble: Enabling the exploration of climate system variability. *Journal of Advances in Modeling Earth Systems*, 11(7), 2050–2069. <https://doi.org/10.1029/2019ms001639>
- Marcos, M., Marzeion, B., Dangendorf, S., Slangen, A., Palanisamy, H., & Fenoglio-Marc, L. (2017). Internal variability versus anthropogenic forcing on sea-level and its components. In *Integrative study of the mean sea-level and its components* (pp. 337–356). Springer.
- Marzeion, B., Cogley, J. G., Richter, K., & Parkes, D. (2014). Attribution of global glacier mass loss to anthropogenic and natural causes. *Science*, 345(6199), 919–921. <https://doi.org/10.1126/science.1254702>
- McCreary, J. P., Han, W., Shankar, D., & Shetye, S. R. (1996). Dynamics of the east India coastal current: 2. Numerical solutions. *Journal of Geophysical Research*, 101(C6), 13993–14010. <https://doi.org/10.1029/96jc00560>
- McDougall, T. J., & Barker, P. M. (2011). Getting started with TEOS-10 and the Gibbs Seawater (GSW) oceanographic toolbox [Dataset]. SCOR/IAPSO WG, 127, 1–28. Retrieved from <https://www.teos-10.org/software.htm>
- McPhaden, M. J., Zebiak, S. E., & Glantz, M. H. (2006). ENSO as an integrating concept in earth science. *Science*, 314(5806), 1740–1745. <https://doi.org/10.1126/science.1132588>
- Meyssignac, B., Salas y Melia, D., Becker, M., Llovel, W., & Cazenave, A. (2012). Tropical Pacific spatial trend patterns in observed sea-level: Internal variability and/or anthropogenic signature? *Climate of the Past*, 8(2), 787–802. <https://doi.org/10.5194/cp-8-787-2012>
- Milne, G. A., Gehrels, W. R., Hughes, C. W., & Tamisiea, M. E. (2009). Identifying the causes of sea-level change. *Nature Geoscience*, 2(7), 471–478. <https://doi.org/10.1038/ngeo544>
- Nidheesh, A. G., Lengaigine, M., Vialard, J., Izumo, T., Unnikrishnan, A. S., & Krishnan, R. (2019). Natural decadal sea-level variability in the Indian Ocean: Lessons from CMIP models. *Climate Dynamics*, 53(9–10), 5653–5673. <https://doi.org/10.1007/s00382-019-04885-z>
- Oliver, E. C. J., & Thompson, K. R. (2010). Madden-Julian Oscillation and sea-level: Local and remote forcing. *Journal of Geophysical Research*, 115(C1). <https://doi.org/10.1029/2009jc005337>
- Park, I. H., Yeh, S. W., Min, S. K., & Son, S. W. (2022). Emergent constraints on future expansion of the Indo-Pacific warm pool. *Geophysical Research Letters*, 49(1), e2021GL097343. <https://doi.org/10.1029/2021gl097343>
- Park, J. Y., Schloesser, F., Timmermann, A., Choudhury, D., Lee, J. Y., & Nellikkattil, A. B. (2023). Future sea-level projections with a coupled atmosphere-ocean-ice-sheet model. *Nature Communications*, 14(1), 636. <https://doi.org/10.1038/s41467-023-36051-9>
- Piecuch, C. G., & Ponte, R. M. (2011). Mechanisms of interannual steric sea-level variability. *Geophysical Research Letters*, 38(15), L15605. <https://doi.org/10.1029/2011gl048440>
- Piecuch, C. G., Thompson, P. R., Ponte, R. M., Merrifield, M. A., & Hamlington, B. D. (2019). What caused recent shifts in tropical Pacific decadal sea-level trends? *Journal of Geophysical Research: Oceans*, 124(11), 7575–7590. <https://doi.org/10.1029/2019jc015339>
- Ponte, R. M. (1994). Understanding the relation between wind-and pressure-driven sea-level variability. *Journal of Geophysical Research*, 99(C4), 8033–8039. <https://doi.org/10.1029/94jc00217>
- Qu, Y., Jevrejeva, S., Williams, J., & Moore, J. C. (2022). Drivers for seasonal variability in sea-level around the China seas. *Global and Planetary Change*, 213, 103819. <https://doi.org/10.1016/j.gloplacha.2022.103819>
- Rayner, N. A. A., Parker, D. E., Horton, E. B., Folland, C. K., Alexander, L. V., Rowell, D. P., et al. (2003). Global analyses of sea surface temperature, sea ice, and night marine air temperature since the late nineteenth century [Dataset]. *Journal of Geophysical Research*, 108(D14), 4407. <https://doi.org/10.1029/2002jd002670>
- Ribes, A., Gillett, N. P., & Zwiers, F. W. (2015). Designing detection and attribution simulations for CMIP6 to optimize the estimation of greenhouse gas-induced warming. *Journal of Climate*, 28(8), 3435–3438. <https://doi.org/10.1175/jcli-d-14-00691.1>
- Richter, K., & Marzeion, B. (2014). Earliest local emergence of forced dynamic and steric sea-level trends in climate models. *Environmental Research Letters*, 9(11), 114009. <https://doi.org/10.1088/1748-9326/9/11/114009>
- Richter, K., Meyssignac, B., Slangen, A. B., Melet, A., Church, J. A., Fettweis, X., et al. (2020). Detecting a forced signal in satellite-era sea-level change. *Environmental Research Letters*, 15(9), 094079. <https://doi.org/10.1088/1748-9326/ab986e>
- Richter, K., Riva, R. E. M., & Drange, H. (2013). Impact of self-attraction and loading effects induced by shelf mass loading on projected regional sea-level rise. *Geophysical Research Letters*, 40(6), 1144–1148. <https://doi.org/10.1002/grl.50265>

- Roxy, M. K., Dasgupta, P., McPhaden, M. J., Suematsu, T., Zhang, C., & Kim, D. (2019). Twofold expansion of the Indo-Pacific warm pool warps the MJO life cycle. *Nature*, *575*(7784), 647–651. <https://doi.org/10.1038/s41586-019-1764-4>
- Roxy, M. K., Ritika, K., Terray, P., & Masson, S. (2014). The curious case of Indian Ocean warming. *Journal of Climate*, *27*(22), 8501–8509. <https://doi.org/10.1175/jcli-d-14-00471.1>
- Sajidh, C. K., & Chatterjee, A. (2023). Indian Ocean dynamic sea-level, its variability and projections in CMIP6 models. *Climate Dynamics*, *61*(5–6), 1–24. <https://doi.org/10.1007/s00382-023-06676-z>
- Samanta, D., Goodkin, N. F., & Karnauskas, K. B. (2021). Volume and heat transport in the South China Sea and maritime continent at present and the end of the 21st century. *Journal of Geophysical Research: Oceans*, *126*(9), e2020JC016901. <https://doi.org/10.1029/2020jc016901>
- Samanta, D., Hameed, S. N., Jin, D., Thilakan, V., Ganai, M., Rao, S. A., & Deshpande, M. (2018). Impact of a narrow coastal Bay of Bengal sea surface temperature front on an Indian summer monsoon simulation. *Scientific Reports*, *8*(1), 1–12. <https://doi.org/10.1038/s41598-018-35735-3>
- Samanta, D., Karnauskas, K. B., & Goodkin, N. F. (2019). Tropical Pacific SST and ITCZ biases in climate models: Double trouble for future rainfall projections? *Geophysical Research Letters*, *46*(4), 2242–2252. <https://doi.org/10.1029/2018gl081363>
- Samanta, D., Karnauskas, K. B., Goodkin, N. F., Coats, S., Smerdon, J. E., & Zhang, L. (2018). Coupled model biases breed spurious low-frequency variability in the tropical Pacific Ocean. *Geophysical Research Letters*, *45*(19), 10–609. <https://doi.org/10.1029/2018gl079455>
- Scafetta, N. (2014). Multi-scale dynamical analysis (MSDA) of sea-level records versus PDO, AMO, and NAO indexes. *Climate Dynamics*, *43*(1), 175–192.
- Sen Gupta, A., Jourdain, N. C., Brown, J. N., & Monselesan, D. (2013). Climate drift in the CMIP5 models. *Journal of Climate*, *26*(21), 8597–8615. <https://doi.org/10.1175/jcli-d-12-00521.1>
- Shaw, P. T., & Chao, S. Y. (1994). Surface circulation in the South China Sea. *Deep Sea Research Part I: Oceanographic Research Papers*, *41*(11–12), 1663–1683. [https://doi.org/10.1016/0967-0637\(94\)90067-1](https://doi.org/10.1016/0967-0637(94)90067-1)
- Slangen, A. B., Church, J. A., Agosta, C., Fettweis, X., Marzeion, B., & Richter, K. (2016). Anthropogenic forcing dominates global mean sea-level rise since 1970. *Nature Climate Change*, *6*(7), 701–705. <https://doi.org/10.1038/nclimate2991>
- Slangen, A. B., Church, J. A., Zhang, X., & Monselesan, D. (2014). Detection and attribution of global mean thermohaline sea-level change. *Geophysical Research Letters*, *41*(16), 5951–5959. <https://doi.org/10.1002/2014gl061356>
- Stammer, D., Cazenave, A., Ponte, R. M., & Tamisiea, M. E. (2013). Causes for contemporary regional sea-level changes. *Annual Review of Marine Science*, *5*(1), 21–46. <https://doi.org/10.1146/annurev-marine-121211-172406>
- Stott, P. A., Gillett, N. P., Hegerl, G. C., Karoly, D. J., Stone, D. A., Zhang, X., & Zwiers, F. (2010). Detection and attribution of climate change: A regional perspective. *Wiley Interdisciplinary Reviews: Climate Change*, *1*(2), 192–211. <https://doi.org/10.1002/wcc.34>
- Sueyoshi, M., & Yasuda, T. (2012). Inter-model variability of projected sea-level changes in the western North Pacific in CMIP3 coupled climate models. *Journal of Oceanography*, *68*(4), 533–543. <https://doi.org/10.1007/s10872-012-0117-9>
- Swart, N. C., Cole, J. N., Kharin, V. V., Lazare, M., Scinocca, J. F., Gillett, N. P., et al. (2019). The Canadian Earth System Model version 5 (CanESM5.0.3). *Geoscientific Model Development*, *12*(11), 4823–4873. <https://doi.org/10.5194/gmd-12-4823-2019>
- Tay, C., Lindsey, E. O., Chin, S. T., McCaughey, J. W., Bekeart, D., Nguyen, M., et al. (2022). Sea-level rise from land subsidence in major coastal cities. *Nature Sustainability*, *5*(12), 1–9. <https://doi.org/10.1038/s41893-022-00947-z>
- Tierney, J. E., Poulsen, C. J., Montañez, I. P., Bhattacharya, T., Feng, R., Ford, H. L., et al. (2020). Past climates inform our future. *Science*, *370*(6517), eaay3701. <https://doi.org/10.1126/science.aay3701>
- Timmermann, A., McGregor, S., & Jin, F. F. (2010). Wind effects on past and future regional sea-level trends in the southern Indo-Pacific. *Journal of Climate*, *23*(16), 4429–4437. <https://doi.org/10.1175/2010jcli3519.1>
- Tokarska, K. B., Hegerl, G. C., Schurer, A. P., Ribes, A., & Fasullo, J. T. (2019). Quantifying human contributions to past and future ocean warming and thermohaline sea-level rise. *Environmental Research Letters*, *14*(7), 074020. <https://doi.org/10.1088/1748-9326/ab23c1>
- Topál, D., Ding, Q., Ballinger, T. J., Hanna, E., Fettweis, X., Li, Z., & Pieczka, I. (2022). Discrepancies between observations and climate models of large-scale wind-driven Greenland melt influence sea-level rise projections. *Nature Communications*, *13*(1), 6833. <https://doi.org/10.1038/s41467-022-34414-2>
- Ushijima, Y., Tsujino, H., Sakamoto, K., Ishii, M., Koshiro, T., & Oshima, N. (2022). Effects of anthropogenic forcings on multidecadal variability of the sea-level around the Japanese coast simulated by MRI-ESM2.0 for CMIP6. *Geophysical Research Letters*, *49*(18), e2022GL099987. <https://doi.org/10.1029/2022gl099987>
- Vialard, J., Shenoi, S. S. C., McCreary, J. P., Shankar, D., Durand, F., Fernando, V., & Shetye, S. R. (2009). Intraseasonal response of the northern Indian Ocean coastal waveguide to the Madden-Julian Oscillation. *Geophysical Research Letters*, *36*(14), L14606. <https://doi.org/10.1029/2009gl038450>
- Voldoire, A., Saint-Martin, D., Sénési, S., Decharme, B., Alias, A., Chevallier, M., et al. (2019). Evaluation of CMIP6 deck experiments with CNRM-CM6-1. *Journal of Advances in Modeling Earth Systems*, *11*(7), 2177–2213. <https://doi.org/10.1029/2019ms001683>
- Walker, J. S., Kopp, R. E., Little, C. M., & Horton, B. P. (2022). Timing of emergence of modern rates of sea-level rise by 1863. *Nature Communications*, *13*(1), 1–8. <https://doi.org/10.1038/s41467-022-28564-6>
- Walker, J. S., Kopp, R. E., Shaw, T. A., Cahill, N., Khan, N. S., Barber, D. C., et al. (2021). Common Era sea-level budgets along the US Atlantic coast. *Nature Communications*, *12*(1), 1–10. <https://doi.org/10.1038/s41467-021-22079-2>
- Warszawski, L., Frieler, K., Huber, V., Piontek, F., Serdeczny, O., Zhang, X., et al. (2017). Center for International Earth Science Information Network—CIESIN—Columbia University. (2016). Gridded population of the World, Version 4 (GPWv4): Population density. Palisades, NY: NASA Socioeconomic Data and Applications Center (SEDAC) [Dataset]. <https://doi.org/10.7927/H4NP22DQ>. Atlas of Environmental Risks Facing China Under Climate Change, 228. Retrieved from <https://sedac.ciesin.columbia.edu/data/set/gpw-v4-population-density-rev11/data-download>
- Weller, E., Min, S. K., Cai, W., Zwiers, F. W., Kim, Y. H., & Lee, D. (2016). Human-caused Indo-Pacific warm pool expansion. *Science Advances*, *2*(7), e1501719. <https://doi.org/10.1126/sciadv.1501719>
- Wills, R. C., Dong, Y., Proistosescu, C., Armour, K. C., & Battisti, D. S. (2022). Systematic climate model biases in the large-scale patterns of recent sea-surface temperature and sea-level pressure change. *Geophysical Research Letters*, *49*(17), e2022GL100011. <https://doi.org/10.1029/2022gl100011>
- Yin, J., Griffies, S. M., & Stouffer, R. J. (2010). Spatial variability of sea-level rise in twenty-first century projections. *Journal of Climate*, *23*(17), 4585–4607. <https://doi.org/10.1175/2010jcli3533.1>

- Yu, B., Li, G., Chen, S., & Lin, H. (2020). The role of internal variability in climate change projections of North American surface air temperature and temperature extremes in CanESM2 large ensemble simulations. *Climate Dynamics*, 55(3–4), 869–885. <https://doi.org/10.1007/s00382-020-05296-1>
- Zhang, L., Han, W., Karlsruhas, K. B., Meehl, G. A., Hu, A., Rosenbloom, N., & Shinoda, T. (2019). Indian Ocean warming trend reduces Pacific warming response to anthropogenic greenhouse gases: An interbasin thermostat mechanism. *Geophysical Research Letters*, 46(19), 10882–10890. <https://doi.org/10.1029/2019gl084088>
- Zhang, X., Lu, Y., & Thompson, K. R. (2009). Sea-level variations in the tropical pacific ocean and the Madden–Julian Oscillation. *Journal of Physical Oceanography*, 39(8), 1984–1992. <https://doi.org/10.1175/2009jpo4170.1>
- Zheng, X. T., Xie, S. P., Du, Y., Liu, L., Huang, G., & Liu, Q. (2013). Indian Ocean Dipole response to global warming in the CMIP5 multimodel ensemble. *Journal of Climate*, 26(16), 6067–6080. <https://doi.org/10.1175/jcli-d-12-00638.1>